Desalination and Water Treatment
www.deswater.com

doi: 10.5004/dwt.2023.29758

303 (2023) 200–211
August

Synthesis and characterization of polymetallic Fe-Co-Ni-S nanocomposite displaying high adsorption capacity for Rhodamine B dye

Bai Sun[a,b,*], Fengshou Zhao[a], Yunming Cheng[a], Chenxu Shao[a], Menghao Sun[a], Mingjian Yi[a], Yun Wang[a], Xiangxiang Wang[a], Shuguang Zhu[a], Xinli Cai[a,*]

[a]*Anhui Institute of Urban and Rural Green Development and Urban Renewal, College of Environment and Energy Engineering, Anhui Jianzhu University, Hefei 230601, China, Tel.: +86-551-63828252; Fax: +86-551-63828252; emails: bsun@mail.ustc.edu.cn (B. Sun), ahcxl@163.com (X. Cai), 1132959870@qq.com (F. Zhao), 502283466@qq.com (Y. Cheng), 2624575993@qq.com (C. Shao), 1343695583@qq.com (M. Sun), mjyi@ustc.edu.cn (M. Yi), 596820989@qq.com (Y. Wang), 350992818@qq.com (X. Wang), zhushuguang@ahjzu.edu.cn (S. Zhu)*

[b]*Environmental Materials and Pollution Control Laboratory, Hefei Institute of Physical Science, Chinese Academy of Sciences, Hefei 230031, China*

Received 14 Janaury 2023; Accepted 3 July 2023

ABSTRACT

Fe-Co-Ni-S (FCNS) nanocomposite is prepared through a hydrothermal method as a new efficient adsorbent to remove organic dyes in wastewater. The morphology, elemental composition and crystalline structure of the adsorbents have been studied by scanning electron microscopy, energy-dispersive X-ray spectroscopy and X-ray diffraction. The influence of the dosage of adsorbent and the pH value on the adsorption performance, the reusability of the nanocomposite, and effects of different anions are studied, which show that the adsorption rate of FCNS towards Rhodamine B (RhB) is as high as 99.63%. The adsorption kinetics of RhB on FCNS is described to pseudo-second-order model. At 318 K, the saturated adsorption capacity is 581.4 mg/g, which is consistent with the Langmuir isotherm. The kinetic results indicate that the adsorption process involves three steps, among which chemical adsorption and intraparticle diffusion play important roles. In addition, through the thermodynamic fitting of the adsorption process, it indicates that the adsorption of RhB by FCNS is spontaneous and accompanied by endothermic reaction. The FCNS nanocomposites has good adsorption performance under pH values ranging from 3 to 11. The FCNS has good reusability and adsorption performance after being reused 5 times. The Fourier-transform infrared spectrum indicates that hydrogen bonding is one of the main factors for influencing the adsorption. Compared with monometallic or bimetallic sulfides, the composite presented here has better adsorption performance and higher adsorption capacity, which will inspire some other emerging trimetallic sulfide composites for various advanced applications.

Keywords: Fe-Co-Ni-S; Adsorption; Nanocomposite; Rhodamine B

1. Introduction

The textile industry generates a large amount of dye wastewater, which is almost half of the globally available dye wastewater [1]. There are over 100,000 different types of commercial dyes, producing more than 7×10^5 tons/y [2]. More than 15% of these basic dyes enter wastewater during the coloring process [3]. Dye wastewater has the characteristics of complex composition, high concentration, large changes in water quality and quantity, strong pH value,

* Corresponding author.

high organic matter content, high color, and high toxicity [4]. Dyes are mutagenic, sensitizing, carcinogenic and non-degradable in water, and also have important effects on ecosystems and human health [5]. Rhodamine B (RhB) is a cationic artificial xanthine dye commonly used in the textile, paper, and food industries [6]. Therefore, considering the harmful and harmful effects of RhB, wastewater contaminated with RhB should be treated before being released into the environment.

The common methods for removing dyes in water include coagulation [7], electrolysis [8], biodegradation [9], membrane separation [10], advanced oxidation [11] and adsorption [12], etc. Compared with other treatments, adsorption is a non-destructive method, which is widely used in wastewater treatment because of its high efficiency and low cost. However, how to find a low-cost, high-efficiency and recyclable adsorbent has become a problem attracting researchers' attention [13]. With the research of nanomaterials, nanomaterials have been proved to be good adsorbents due to their unique morphology and structural characteristics, and can be widely used to remove Rhodamine B from water [14]. Adsorption is easy to handle, non-toxic, and a cost-effective physicochemical method for removing contaminants (e.g., dyes) from industrial wastewater [15–17]. At present, the most commonly used adsorbents are activated carbon [18], clay [19], polymer materials [20] and metal–organic framework [21]. From the perspective of economy and practicality, many researchers need to study a kind of adsorbent with low cost, simple production method and high adsorption efficiency [22]. Fat'hi et al. [23] used almond shell (AS) to remove and recover Acid blue 129 (AB129). When the optimal pH value is 2 and the initial dye concentration is 40 mg/L, the removal rate exceeds 98% within 14 min, and the adsorbent dosage is 0.4 g. Sharifpour et al. [24] used a simple method to prepare CuO-NPs-AC adsorbents doped with cobalt ions. The adsorption isotherms of CuO-NPs-AC doped with minimum for MO and MG can be well clarified through the Langmuir model. The maximum adsorption capacity of a single solution is 320.69 and 290.11 mg/g, and the maximum adsorption capacity in a binary solution is 233.02 and 205.53 mg/g. Arabkhani et al. [25] prepared a new graphite oxide (GO)/sodium montmorillonite (NaMMT) polymer nanocomposite with three-dimensional structure, which has good adsorption performance for malachite green (MG) dye in real wastewater, and the pseudo-second-order kinetic model fits the adsorption process well. Because of its high adsorption activity, Ni-Co-S has become the most optimistic class of efficient sorbents in recent years [26]. The introduction of other non-noble metal elements into Ni-Co-S can further improve its performance [27]. Iron-based nanoparticles are considered a promising candidate because of their strong chemical stability [28]. Bimetallic (Fe and Co) sulfides have been widely studied in the field of wastewater treatment due to their excellent catalytic properties and electron transport capabilities, and have shown broad prospects [29]. Bimetallic (Fe and Ni) sulfides have been widely reported due to their good catalytic properties [30]. Fe-Co-Ni-S (FCNS) nanocomposite exhibits a unique porous network and high synergy [31]. Therefore, it is a good choice to synthesize related composite to achieve an economical and efficient adsorbent for removing RhB in water.

Herein, FCNS nanocomposite is synthesized by a simple hydrothermal method. RhB, which is widely available in industrial wastewater, was chosen to model xanthine contamination. The adsorption characteristics during RhB removal have been analyzed by adsorption kinetics, isotherms and thermodynamic models. Scanning electron microscopy (SEM), X-ray diffraction (XRD) and energy-dispersive X-ray spectroscopy (EDS) are used to study the morphology and elemental composition of the adsorbent. Compared with monometallic or bimetallic sulfides, the results show that FCNS nanocomposite has better adsorption performance and higher adsorption capacity than previous adsorption experiments, which will inspire some other emerging trimetallic sulfide composites for various advanced applications. The adsorption mechanism has also been analyzed by Fourier-transform infrared spectroscopy (FTIR). The influence of pH, and dosage of adsorbent on the adsorption performance are studied to get the best experimental conditions.

2. Experimental set-up

2.1. Reagents and instruments

The reagents used in the experiment mainly include sodium chloride (NaCl, 99.7%), sodium nitrate ($NaNO_3$, 99.7%), sodium sulfate (Na_2SO_4, 99.7%), sodium dihydrogen phosphate (NaH_2PO_4, 99.7%), nickel chloride hexahydrate ($NiCl_2{\cdot}6H_2O$, 98.0%), cobalt dichloride tetrahydrate ($CoCl_2{\cdot}4H_2O$, 99.7%), urea ($CO(NH_2)_2$, 99.0%), ferrous sulfate heptahydrate ($FeSO_4{\cdot}7H_2O$, 98.0%) and sodium thiosulfate pentahydrate ($Na_2S_2O_3{\cdot}5H_2O$, 99.0%) were purchased from Sinopharm Chemical Reagent Co., Ltd., (Shanghai, China) and used as received without further purification. Anhydrous ethanol (C_2H_6O, 99.7%), analytical purity, Xilong Scientific Co., Ltd., (Guangdong, China). Deionized water is prepared by FST-TOP-A24 super pure water equipment by Shanghai Fushite Instrument Equipment Co., Ltd., (Shanghai, China).

The instruments used in the experiment mainly include: DHG-9023A air drying box, Shanghai Yiheng Scientific Instrument Co., Ltd., (Shanghai, China). PHS-3C digital pH meter, Shanghai Yidian Scientific Instrument Co., Ltd., (Shanghai, China). PTFE reaction kettle, Shanghai Jinghong Experimental Equipment Co., Ltd., (Shanghai, China). FA2204N electronic balance, Shanghai Jinghai instrument Co., Ltd., (Shanghai, China). TG16K-II Table high-speed centrifuge, Shanghai ZhaoDi bio-technology Co., Ltd., (Shanghai, China).

2.2. Preparation of adsorbent

FCNS nanocomposite was synthesized by using a hydrothermal method. The preparation process was as follows: $FeSO_4{\cdot}7H_2O$ (0.28 g, 1 mM), $CoCl_2{\cdot}4H_2O$ (0.20 g 1 mM) and $NiCl_2{\cdot}6H_2O$ (0.24 g, 1 mM) were dissolved in 20 mL deionized water, and stirred for 30 min until completely dissolved. Then $Na_2S_2O_3{\cdot}5H_2O$ (0.25 g, 1 mM) was added to the above solution and kept stirring for 1 h until evenly mixed. The homogeneous solution was transferred to a Teflon-lined stainless-steel autoclave and heated in an oven at 180°C for

12 h. After cooling to room temperature, the obtained solid products were centrifuged and washed three times with deionized water and ethanol, respectively, and then vacuum dried at 60°C for 12 h to prepare FCNS sample. For comparison, Fe-Co-S (FCS) nanocomposite and Fe-Ni-S (FNS) nanocomposite were synthesized via the same procedure without the addition of $Ni(Cl)_2{\cdot}6H_2O$ and $Co(Cl)_2{\cdot}4H_2O$, denoted as FCS nanocomposite and FNS nanocomposite, respectively.

2.3. Characterization

The surface morphology and structure of FCNS nanocomposite was characterized by field emission scanning electron microscopy (SEM, AURIGA, ZEISS Company, Germany) coupled with an energy dispersive spectrometer (EDS, INCA X-Max 50, ZEISS Company, Germany). The X-ray diffractometer (XRD, PANalytical, Netherlands) with a Cu Kα source was used to analyze the crystalline structure. Fourier-transform infrared spectroscopy (FTIR, Nexus-870, Thermo Nicolet, USA) was used to determine the change of surface properties. The wavelength change of the adsorbent was recorded by UV-2600i UV-Vis spectrophotometer (UV-2600i, UV-Vis, Shimadzu, China).

2.4. Batch adsorption experiments

Batch experiments were conducted in 250 mL cones. Briefly, the particles were dispersed in an aqueous solution (100 mL, 10 mg/L, temperature = 298 K, pH = 7) and oscillated in the dark for 12 h. At predetermined time intervals, an aliquot (2 mL) of the reaction solution was removed quickly to filter through a 0.22 μm syringe filter into a tube to measure the absorbance. By comparing the removal rate, the excellent adsorption performance of RhB by FCNS nanocomposite was characterized. Batch experiments to explore initial pH, adsorption dose and regeneration performance were carried out under the same conditions. All experiments were performed in duplicates and average values with standard deviations were reported.

2.4.1. Preparation of RhB standard solution

25 mg of RhB was dissolved in 100 mL of deionized water, sonicated for 15 min, and transferred to a 250 mL volumetric flask to complete constant volume, that is, 100 mg/L of RhB standard solution. RhB solution in all adsorption experiments was obtained by diluting the standard solution with deionized water. Prepared RhB solution with concentration gradient of 5, 10, 20, 30, 40, 50 and 60 mg/L, and measured its absorbance at 554 nm wavelength by ultraviolet spectrophotometer. Then the RhB standard curve was obtained by linear regression analysis of the concentration and absorbance of RhB.

2.4.2. Calculation of adsorption capacity and removal rate

Untreated dye wastewater was simulated by employing different concentrations of RhB solution. The 20 mg FCNS nanocomposite was added to 100 mL, 10 mg/L RhB solution for batch adsorption experiments. The whole experiment was carried out in a constant temperature oscillation chamber with shading, with the room temperature set at 298 K and the rotation speed at 160 rpm. After waiting for the adsorption equilibrium, the absorption value at 554 nm absorption wavelength was measured by UV-Vis. The effect of adsorbent dose and initial pH on experiment was studied by the same experimental method, and its isothermal line and kinetics were analyzed. The dye removal rate (%) and the amount of dye adsorption were calculated by Eqs. (1) and (2), respectively.

$$\eta = \frac{\left(C_0 - C_e\right)}{C_0} \times 100\% \tag{1}$$

$$q_e = \frac{\left(C_0 - C_e\right) \times V}{m} \tag{2}$$

where C_0 (mg/L) and C_e (mg/L) were the initial concentration before adding the adsorbent and the equilibrium concentration after adding the adsorbent, respectively; q_e (mg/g) was the adsorption capacity at the adsorption equilibrium; V (L) was the volume of RhB solution; m (g) was the dosage of adsorbent; η is the removal rate of the adsorbent.

2.4.3. Study on adsorption isotherms

In the study of adsorption isotherm of FCNS on RhB, take 100 mL of RhB solution with concentration of 10, 20, 30, 40, 50, 60, 70 and 80 mg/L, 20 mg of FCNS was added to it respectively, and then put 250 mL conical flask filled with RhB solution and adsorbent into a constant temperature shaker for shading and shaking for 12 h (298 K, 160 rpm). After the end of oscillation, conduct high-speed centrifugation, take an appropriate amount of supernatant, and pass through 0.22 μM inorganic filter membrane, and the absorbance value was measured by UV-Vis.

2.4.4. Study on adsorption thermodynamics

In the study of adsorption thermodynamics, at 298, 308 and 318 K, respectively, the vibration frequency of 160 rpm was oscillated in a constant temperature shaker for 12 h. After the oscillation, centrifuge and filter, measure the absorbance value of RhB solution at the absorption wavelength of 554 nm, and finally analyze the data to obtain the entropy change, enthalpy change and Gibbs free energy change of the adsorption experiment.

2.4.5. Study on adsorption kinetics

20 mg of adsorbent was added to 100 mL of RhB solution with a concentration of 10 mg/L, and the solution was shielded from light and stirred. First, take samples at 2, 4, 6, 8, 10, 15 and 30 min, respectively.

2.4.6. Effect of adsorbent dosage

5, 10, 15, 20, 25, 30 and 35 mg of adsorbents were added to 100 mL of RhB solution with a concentration of 10 mg/L, respectively. Then, shaking them for 12 h under shading.

Taking samples for measurement to explore the effect of the amount of adsorbent on the adsorption performance.

2.4.7. Effect of pH

0.1 mol/L HCl and 1 mol/L NaOH solution were used to adjust the pH value of 100 mL RhB solution with a concentration of 10 mg/L. The pH value range of the solution was set to 3–11. Then, 20 mg of adsorbent was added, respectively, and the effect of pH on the adsorption performance was investigated by shading and shaking for 12 h.

2.4.8. Study on regeneration capacity of adsorbent

In order to evaluate the regeneration ability of the adsorbent, pour a certain amount of saturated adsorbent into 0.1 mol/L NaOH solution for desorption and reuse. Repeat the five cycle regeneration experiments to explore the regeneration performance of FCNS.

2.4.9. Effect of coexisting anions

Four inorganic salts (NaCl, $NaNO_3$, Na_2SO_4, and NaH_2PO_4) with concentrations ranging from 0 to 10 mmol were selected to investigate the effect of coexisting ions on the adsorption and removal of RhB by the adsorbent. The experiment used a series of 100 mL RhB solutions with an initial concentration of 10 mg/L. Adjust pH = 7 and add 20 mg of adsorbent. It was put in a constant temperature oscillator to avoid light oscillation and absorb for 12 h (298 K, 160 rpm). The absorbance of the supernatant was measured after filtering with the membrane, and the RhB concentration was calculated based on the standard curve. Three parallel experiments were conducted to explore the effect of coexisting ions on adsorption performance.

3. Results and discussion

3.1. Sample characterization

Fig. 1a–d display the SEM images of FCNS before and after adsorption of RhB. It can be seen from Fig. 1a and b that FCNS sample presents some small spherical morphology structures. The particles are aggregated and distributed evenly, and there are large gaps between the particles. From Fig. 1c and d it can be seen that obvious aggregates on the surface of the material, which shows that RhB dye is adsorbed in the gaps and surfaces of adsorbent particles, indicating that the material has adsorption for RhB. The RhB solution adheres to the surface of the material after adsorption, and the shape of the material becomes irregular. Therefore, the surface of the adsorbent changes after the adsorption of RhB. A similar phenomenon was reported by Jia et al. who reported that the residue of RhB on the surface has a significant effect on the morphology [32].

In order to investigate the elemental composition and content of FCNS, the adsorbent was characterized by EDS. Table 1 lists the contents of various elements adsorbent, of which the sulfate element content accounts for the largest proportion. In addition, it can be seen from the table that

Table 1
Elemental content of FCNS adsorbent

Element	Atomic %
S K	55.04
Fe K	4.25
Co K	11.11
Ni K	29.6
Total	100

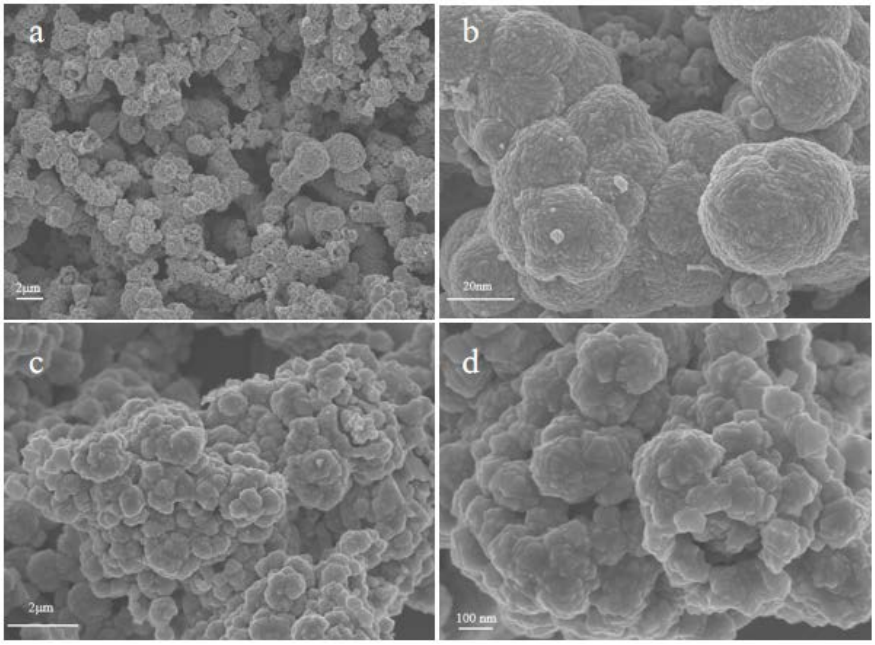

Fig. 1. (a,b) Scanning electron microscopy images before FCNS adsorption and (c,d) SEM images after FCNS adsorbs RhB solution.

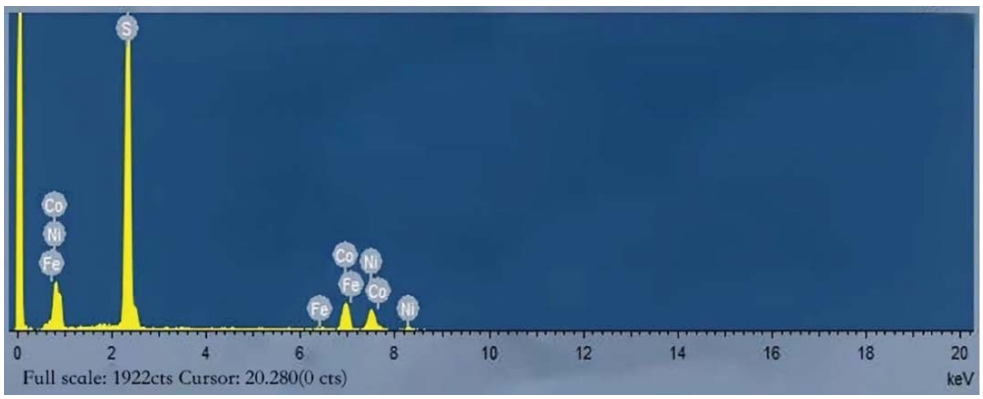

Fig. 2. Energy-dispersive X-ray spectrum of FCNS adsorbent.

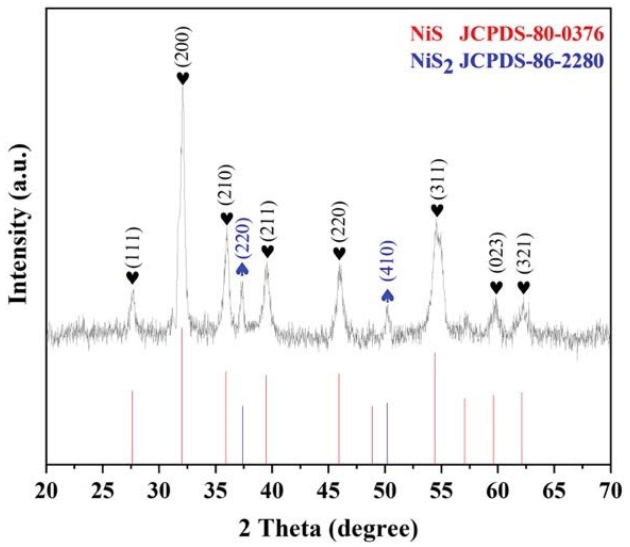

Fig. 3. X-ray diffraction pattern of FCNS.

the composite contains sulfate, nickel, cobalt and iron. The EDS spectrum of FCNS nanocomposites is shown in Fig. 2. The result shows that the composite contains iron, cobalt, nickel and sulfur.

To investigate the crystal structure and phase purity of the adsorbent, XRD analysis of the adsorbent was performed. As shown in Fig. 3, it can be seen that the crystallinity of the FCNS nanocomposite is good. The characteristic diffraction peaks of the adsorbent at 2θ = 27.64°, 32.02°, 35.93°, 39.49°, 45.92°, 54.44°, 59.64° and 62.13° correspond to (111), (200), (210), (211), (220), (311), (023), (321) crystal planes of the NiS_2 (NO.80-0376), respectively. The remaining characteristic peaks located at 2θ = 37.41° and 50.21° correspond to the (220) and (410) crystal planes of the NiS (NO.86-2280). The results of the XRD pattern are consistent with the results in Table 1 for the higher elemental content of Ni and S, and the lower elemental content of EDS for Fe and Co. Combined with the XRD analysis it is clear that no fixed crystalline form was produced for either element. The sample contains less iron and cobalt, indicating that the compounds of iron and cobalt do not form a fixed crystalline form.

3.2. Study on adsorption isotherms and adsorption thermodynamics

Freundlich and Langmuir models were used to investigate the mechanism of the adsorption and to calculate the adsorption capacity [33]. Freundlich and Langmuir models and linear equations were used to study the adsorption performance of FCNS. Eqs. (3) and (4) are usually used to fit experimental results [34]. The corresponding parameters of the two models are shown in Table 2. Thermodynamic parameters can be obtained from Eqs. (5) and (6) [35].

$$\frac{C_e}{q_e} = \frac{C_e}{q_m} + \frac{1}{K_L + q_m} \tag{3}$$

$$\ln q_e = \frac{1}{n}\ln C_e + \ln k_F \tag{4}$$

$$\Delta G = -RT\ln K \tag{5}$$

$$\ln K = -\frac{\Delta H}{RT} + \frac{\Delta S}{R} \tag{6}$$

where C_e (mg/L) is the concentration after equilibrium adsorption; q_e (mg/g) is the adsorption capacity after equilibrium; q_m (mg/g) and K_L (L/mg) are the maximum adsorption capacity and constants calculated by Langmuir equation. K_F (mg/g), n is the adsorption constant of Freundlich equation. R is the general gas constant (8.314 J/(mol·K)), T is the temperature (K); K is the Langmuir adsorption constant of; ΔS is the entropy change; ΔG is the Gibbs free energy change; ΔH is the enthalpy change.

Adsorption isotherm can reflect the distribution characteristics of the adsorbent. It can be seen from Fig. 4a and c that the adsorption effect of FCNS on RhB increases with the increase of temperature. The parameters of the corresponding isotherm model are listed in Table 2. The correlation coefficient indicates that the maximum R^2 of Langmuir model at different temperatures is 0.997, which is greater than the determined coefficient R^2 of Freundlich isotherm model, indicating that Langmuir model can better describe the adsorption process. It is well known that the Langmuir model assumes that the surface of the adsorbent

Table 2
Different adsorption isotherm model parameters for RhB adsorption at different temperatures

Isotherm model	Langmuir $\left(\frac{C_e}{q_e}=\frac{C_e}{q_m}+\frac{1}{K_L q_m}\right)$			Freundlich $\left(\ln q_e=\frac{1}{n}\ln C_e+\ln K_F\right)$		
Parameters	K_L (L/mg)	q_m (mg/g)	R^2	$1/n$	K_F (mg/g)	R^2
298 K	0.0247	526	0.992	0.913	9.79	0.990
308 K	0.0471	546	0.995	0.776	21.0	0.991
318 K	0.157	581	0.997	0.554	59.9	0.987

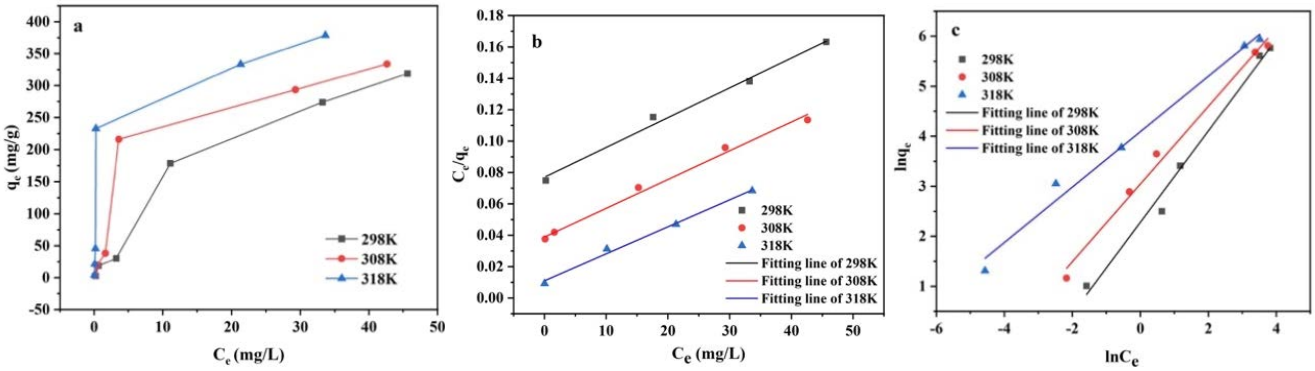

Fig. 4. Adsorption thermodynamics of (a) RhB at different temperatures; the fitting plot of (b) Langmuir model and (c) Freundlich model at different temperatures. Reaction conditions: $[FCNS]_0$ = 20 mg, volume = 100 mL, pH = 7, time = 12 h.

is monolayer and homogeneous, whereas the Freundlich model deduces that the surface is heterogeneous [36]. The results indicate that FCNS nanocomposite carry out monolayer adsorption and the adsorption sites on the adsorbent are evenly distributed. The Langmuir model shows that the saturation adsorption capacity of FCNS nanocomposite can reach 581.4 mg/g. In addition, it can be observed from Table 2 that all values of $1/n$ were between 0 and 1, which again proves that chemisorption occurs for RhB [37]. And it further shows that the adsorption was monolayer adsorption on a homogenous surface. By comparing the adsorption capacity of different adsorbents in Table 3, it can be concluded that FCNS nanocomposite have higher adsorption capacity for RhB compared with other adsorbents.

Thermodynamic analysis of adsorption is essential to understand the adsorption mechanism. Fig. 4a shows that at the same temperature, the equilibrium adsorption capacity of RhB increases depending on the increase of equilibrium concentration. According to Table 2, at the same equilibrium concentration, the increase in temperature will promote the adsorption process to a certain extent, indicating that the adsorption performance of FCNS improves with the increase of temperature. According to Table 4, the negative value of ΔG show that the adsorption process was spontaneous. The value of ΔH was positive, indicating that the adsorption process was endothermic. Similar findings have been reported in the literature [45]. In addition, $\Delta H > 0$ indicates the typical endothermic property of the adsorption process. At the same time $\Delta S > 0$, it means that the chaos and randomness at the interface between adsorbent and adsorbent increase, and the reaction is irreversible, which is conducive to the stability of adsorption [46]. In conclusion, increasing the temperature is conducive to the adsorption.

Table 3
Comparison of adsorption capacity of different adsorbents

Adsorbents	Efficiency (mg/g)	References
$Ni_{0.4}Co_{0.2}Zn_{0.4}Fe_2O_4$ nanocomposite	131.573	[38]
Graphene oxide–silica composite	333.33	[39]
$NiCo_2O_4$	366	[40]
C/MnCuAl-LDOs	317.2	[41]
IZO	171	[42]
Fe_3O_4@C	262.72	[43]
$Fe_xCo_{3-x}O_4$	128.6	[44]
FeCoNiS	581.4	This work

3.3. Adsorption kinetic study

In order to further understand the relationship between the structure of the adsorbent and the adsorption form, the adsorption rate and adsorption efficiency of the adsorbent to the adsorbate molecules are described by using two pseudo-first-order and pseudo-second-order kinetic models to explore the adsorption kinetics of the whole adsorption process [47]. Pseudo-first-order kinetic model, pseudo-second-order kinetic model, and particle intima diffusion model were fitted and calculated by Eqs. (7)–(9), respectively:

$$\ln\left(q_e - q_t\right) = \ln q_e - \frac{k_1 t}{2.303} \tag{7}$$

$$\frac{t}{q_t} = \frac{1}{k_2 q_e^2} + \frac{t}{q_e} \tag{8}$$

$$Q_t = K_{ip} t^{1/2} + C \tag{9}$$

where q_e and q_t (mg/g) are the amount of TC adsorbed at equilibrium and at a certain time, respectively; t (min) is the adsorption time; k_1 (min^{-1}) and k_2 (g/(mg·min)) are the rate constants of pseudo-first-order and pseudo-second-order reactions, respectively; K_{ip} (mg/g·min$^{1/2}$) is the intraparticle diffusion model constant, and C (mg/g) is a constant to describe the boundary layer thickness.

Fig. 5a and c show the kinetic model fitting the adsorption process of FCNS for RhB in a certain time. The adsorption is divided into three stages: Firstly, during the shaking process, the adsorption sites on the surface of the FCNS nanocomposite contact RhB, and the reaction speed increases. Secondly, the adsorption leads to the gradual saturation of the adsorption sites on the adsorbent surface, which further reduces the adsorption rate. Finally, the adsorption amount reaches saturation. To investigate the adsorption mechanism, the adsorption kinetics of RhB dye on FCNS nanocomposite was studied by pseudo-first-order and pseudo-second-order kinetic models [48]. The data were processed by Eqs. (7) and (8) and linearly fitted to obtain the pseudo-first-order and pseudo-second-order models, as shown in Fig. 4b and c, respectively. The parameters of the two dynamic models obtained by nonlinear regression on the experimental data are shown in Table 5. The fit results showed a pseudo-second-order kinetic model. The coefficient R^2 = 0.999 was greater than that of the pseudo-first-order kinetic model R^2 = 0.992. The pseudo-second-order kinetic model can better describe the adsorption process, which is mainly consistent with chemisorption [49].

In order to obtain more detailed information on the adsorption mechanism and describe the rate influencing steps of RhB adsorption on FCNS, the intraparticle diffusion model was applied, as shown in Eq. (9). The diffusion model fitted in Fig. 5d shows that the color undergoes significant changes over a certain period of time during the adsorption process, exhibiting a continuous stage composing of rapid adsorption, medium adsorption, and equilibrium adsorption [50]. The sharp increase in the first stage is film diffusion, where the adsorbate diffuses towards the surface of the adsorbent (film diffusion) [51]. The second

Table 4
Thermodynamic parameters of FCNS adsorbing RhB

Parameters	T (K)	K_d	ΔG (kJ/mol)	ΔS (kJ/(mol·K))	ΔH (kJ/mol)
FCNS	298	9.78	–5.65	22.3	19.0
	308	13.1	–6.59		
	318	24.3	–8.43		

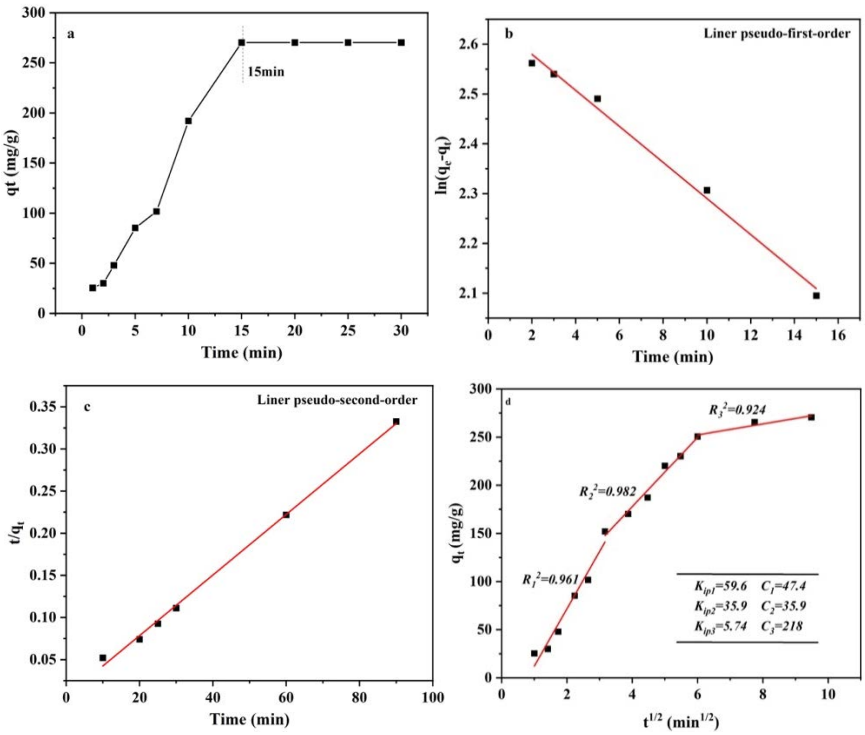

Fig. 5. (a) Kinetic experimental data of RhB adsorption by FCNS nanocomposite, (b) plot for the pseudo-first-order, (c) plot for the pseudo-second-order, and (d) diffusion model of RhB adsorbed by FCNS. Reaction conditions: $[FCNS]_0$ = 20 mg, $[RhB]_0$ = 10 mg/L, volume = 100 mL, temperature = 298 K, pH = 7, time = 12 h.

Table 5
Pseudo-first-order and pseudo-second-order kinetic fitting parameters of FCNS adsorbing RhB

This work	Pseudo-first-order kinetics			Pseudo-second-order kinetics		
q_e (mg/g)	k_1 (1/min)	q_e (mg/g)	R^2	k_2 (g/(mg·min))	q_e (mg/g)	R^2
271	0.0157	14.2	0.992	0.00210	278	0.999

stage is a slow process, where the adsorbate diffuses on the adsorbent (particle diffusion) [52]. The final stage is the equilibrium stage, where RhB is adsorbed onto the inner surface of the adsorbent [53]. In contrast, the adsorption rate is fast within 36 min, and the adsorption process is mainly controlled by the first and second stages, as a large number of RhB molecules occupy a large amount of surface area [50]. Therefore, it can be concluded that the adsorption of RhB on FCNS is controlled by physical adsorption and chemical interactions.

3.4. Effect of adsorbent dosage

It is essential to obtain the optimal dose of sorbent to reduce the waste of resources, so that the optimal absorption capacity can be obtained on a resource efficient basis [54]. When the amount of adsorbent is less than 20 mg, the removal efficiency of RhB by the adsorbent increases quickly, as shown in Fig. 6, because the removal rate increases with the increase of adsorbent, which is due to more adsorption sites. The optimal removal rate can reach 99.63%, while the dosage of FCNS nanocomposite is 20 mg. When the amount of adsorbent continues to increase, the removal rate almost remains unchanged that means that the adsorption reaction reaches an equilibrium state. Because the initial RhB concentration is constant, and the RhB concentration decreases as increasing removal rate. Therefore, increasing the dosage of adsorbent will reduce the RhB adsorption capacity per unit mass of adsorbent [55]. Meanwhile, although the efficiency of RhB removal of FCS nanocomposite and FNS nanocomposite increased with the increase of catalyst dosage, the growth efficiency was far less than that of FCNS nanocomposite, which also indicated that the RhB removal activity of FCS nanocomposite and FNS nanocomposite was not as excellent as that of FCNS nanocomposite. When the adsorbent dose was increased to 35 mg, the reaction still did not reach equilibrium. Combined with the removal rate and economy, it shows that 20 mg of FCNS can basically remove RhB in the solution.

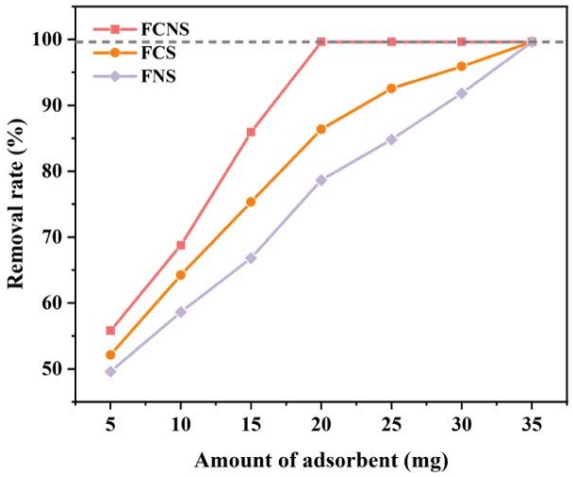

Fig. 6. Effect of FCNS dosage on RhB removal efficiency. Reaction conditions: $[RhB]_0$ = 10 mg/L, volume = 100 mL, pH = 7, temperature = 298 K, time = 12 h.

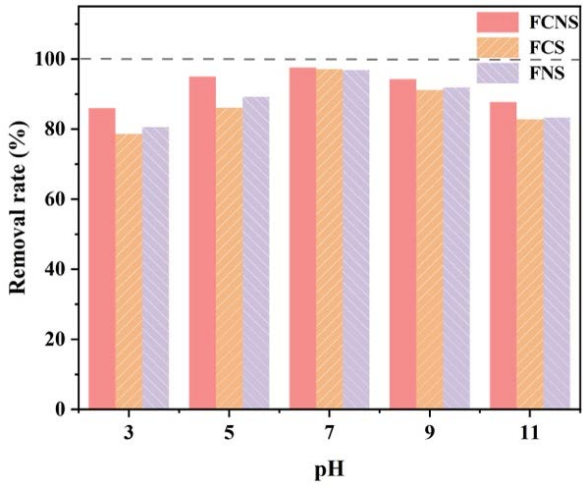

Fig. 7. Effect of pH on removal of RhB by FCNS adsorbent. Reaction conditions: $[FCNS]_0$ = 20 mg, $[RhB]_0$ = 10 mg/L, volume = 100 mL, temperature = 298 K, time = 12 h.

3.5. Effect of pH

The pH value is an important parameter affecting the adsorption of dyes on adsorbents, because the structure of dyes and the chemical properties of adsorbents are highly dependent on the pH value of the solution [56]. It can be seen from Fig. 7 the removal efficiency of the adsorbent for RhB is good and stable under neutral and acidic environmental conditions, which can be maintained at about 96.00%, and can reach 97.56% when pH = 7. However, even in an alkaline atmosphere, compared with FCS nanocomposite and FNS nanocomposite, the removal rate of RhB by FCNS nanocomposite can still reach 87.76%. When pH = 3, the adsorption performance of FCS and FNS nanoparticles decreased significantly, which was speculated to be because they could not exist stably in acidity. However, the stability of FCNS adsorbent composed of polymetal is further enhanced due to the strong interaction between ions. Regarding the effect of pH on the efficiency, there have been studies reported RhB exists as cations and zwitterions

in polar solvents [57]. Li et al. [32] found that when the pH value of the solution was less than 3.0, RhB molecules mainly existed in cationic form (RhB^+). With the further increase of pH value, the RhB component of cationic (RhB^+) decreased, while the RhB component of zwitter ion ($RhB^±$) increased, resulting in the increased adsorption of RhB by FCNS nanocomposite in the range of pH 4~7. At higher pH (pH = 11), the adsorption capacity is significantly reduced due to electrostatic repulsion of negatively charged RhB and negatively charged FCNS nanocomposite. So FCNS nanocomposite has strong practical application potential in adsorption and removal of RhB.

3.6. Study on regeneration capacity of adsorbent

In order to better reduce the cost of applications, the recovery performance of the absorbent is particularly important [58]. When the adsorption equilibrium is reached, the solution was first desorbed with 0.1 mol/L NaOH. The adsorbent was collected by centrifugation, cleaned with deionized water, and the adsorption experiment was repeated for 5 cycles. In Fig. 8, the removal rate of RhB by the adsorbent FCNS nanocomposite can reach 99.63%. Even after 5 cycles, the removal rate can still be maintained at 88.33%. While FCS nanocomposite and FNS nanocomposite show different degrees of reduced adsorption activity, the adsorption rate of FCS nanocomposite and FNS nanocomposite decrease to 78.82% and 71.67%, respectively, indicating that the adsorbent has good reusability and practical application prospect.

3.7. Effect of coexisting anions

In addition, the coexistence of anions (Cl^-, SO_4^{2-}, NO_3^-, and $H_2PO_4^-$) on FCNS adsorption was explored [59], as shown in Fig. 9. The removal rate of RhB decreases with increasing ion concentration, which is due to the competitive effect of the ions added to the solution on the adsorption sites, reducing the binding between the adsorbent and RhB. At the same time, the positive charge on the surface of FCNS is neutralized due to an increase in ion concentration. In addition, the adsorbent has weak ion exchange ability and can exchange ions with strong acids such as SO_4^{2-}, $H_2PO_4^-$, Cl^-, NO_3^-. Among the four coexisting ions, SO_4^{2-} ion has a stronger ability to bind to the basic group of the adsorbent because of its higher negative charge, so SO_4^{2-} has the largest impact on RhB adsorption at the same molar concentration. Cl^-, $H_2PO_4^-$, and NO_3^- show no significant effect on the adsorption of RhB. Therefore, the adsorption of RhB remains at a high level under the influence of coexisting ions with good selectivity.

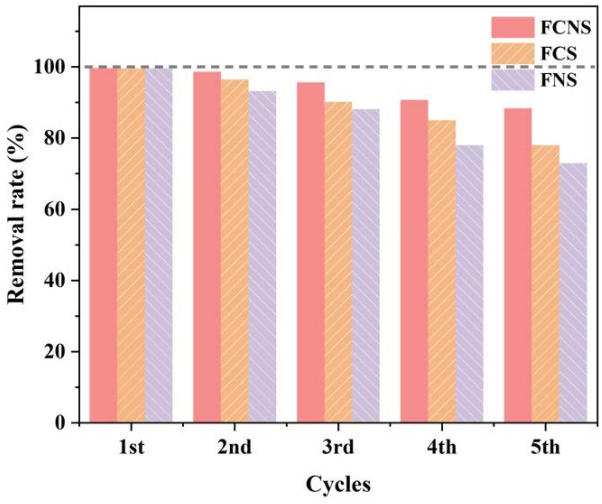

Fig. 8. Regeneration performance of FCNS adsorbent. Reaction conditions: $[FCNS]_0$ = 20 mg, $[RhB]_0$ = 10 mg/L, volume = 100 mL, pH = 7, temperature = 298 K, time = 12 h.

3.8. FTIR analysis

Infrared spectroscopy is widely used to study the structural characteristics of materials. As can be seen from Fig. 10, the wavenumber of the characteristic peaks changed

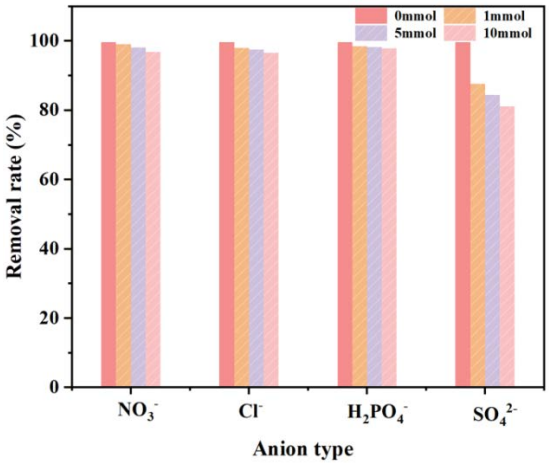

Fig. 9. Effect of coexisting anions and ionic strength on removal of RhB by FCNS. Reaction conditions: $[FCNS]_0$ = 20 mg, $[RhB]_0$ = 10 mg/L, volume = 100 mL, pH = 7, temperature = 298 K, time = 12 h.

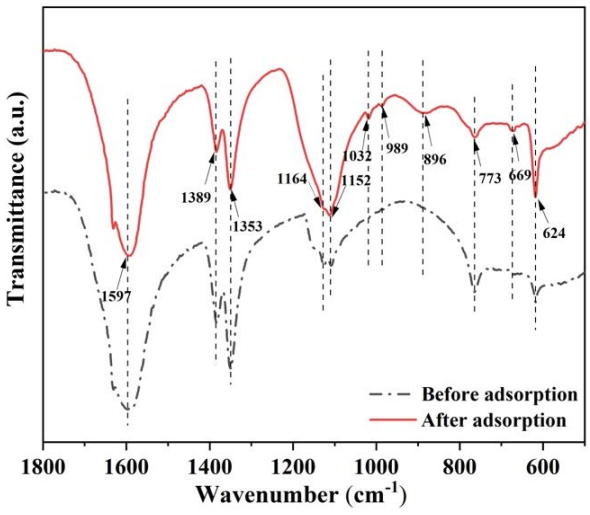

Fig. 10. Fourier-transform infrared spectra of FCNS adsorbent.

before and after adsorption by the adsorbent. Due to water absorption, the low frequency change at 1,597 cm^{-1} can be considered as the bending vibration between H_2O layers [60]. The change from 1,389–1,353 cm^{-1} adsorption is due to O–H bending, especially the O–H and carboxyl groups [61], which indicates an H-bonding interaction between the –OH group on the nanocomposite and the $–NH_2$ or R_3N group of the dye [62]. The 1,164–1,152 cm^{-1} band is attributed to the C=O stretching vibration [63] and presumably due to the skeletal stretching of the aromatic structure [64]. Peaks 1,032 and 989 cm^{-1} almost disappeared after adsorption due to the reduction of C–O bonds [65]. The peak at 896 cm^{-1} became smaller due to the stretching vibration of C–N bonds [66]. The peak change at 773 cm^{-1} may be due to the presence of a C–C bond in the benzene ring after adsorption [67]. Peak at 669 cm^{-1} becomes smaller, presumably due to the stretching vibration of C–H during the adsorption [68]. The Ni–S bond peak at 624 cm^{-1} proves the presence of a sulphide compound [67].

4. Conclusion

In summary, FCNS nanocomposite was synthesized by a simple hydrothermal method, which has good adsorption performance for RhB. The effects of adsorbent dosage, pH value, and different anions on RhB adsorption were studied. The adsorption mechanism of RhB on FCNS Shows that the RhB molecules can freely diffuse between the particle structures of FCNS and bind to functional groups on the surface through hydrogen bonds. At 318 K, the saturated adsorption capacity is as high as 581.4 mg/g. In addition, it is found that the trimetallic sulfides have better adsorption performance than monometallic or bimetallic sulfides. The results of adsorption kinetics and isotherm show that the adsorption conforms to the pseudo-second-order kinetics and Langmuir model, and the adsorption of RhB by the FCNS nanocomposite is dominated by chemical adsorption. The adsorption thermodynamic results show that the adsorption capacity of the adsorbent for RhB increased with the increase of temperature. The thermodynamic parameters $\Delta G < 0$, and both ΔH and ΔS are greater than 0, indicating that the adsorption is endothermic and spontaneous. The FCNS nanocomposite has excellent adsorption capacity for RhB adsorption over a wide range of pH from 3 to 11. From the cyclic adsorption experiment, it shows that after five cycles of use, the removal rate of RhB decreased from 99.63% to 88.33%, and the efficiency decreased by 11.30%. Moreover, FCNS nanocomposite can still maintain high RhB removal efficiency after repeated regeneration with NaOH, and has excellent reusability, which indicates its potential for applications.

Acknowledgments

The authors are especially grateful to the Project of National Key Research and Development Program (2019YFC0408505), 2022 Provincial Quality Engineering Project for Higher Education Institutions of Anhui Province (2022jyxm276), the Natural Science Research Project of the Higher Education Institutions of Anhui Province (KJ2021A0616,KJ2020A0468), the National Natural Science Foundation of China (52103104, 61873003), the Natural Science Foundation of Anhui Province (1908085QE241), the first batch of natural science projects supported by surplus funds in 2021 of Anhui Jianzhu University (JZ202129,JZ202134) and the Scientific Research Start-up Foundation for Introduction of Talent, Anhui Jianzhu University (2016QD113).

References

[1] J.J. Zhang, Z.W. Yang, L.S. Wang, L. Chao, Carbon covered Ag and Bi nanoparticles uniformly dispersed in porous carbon matrix: synergistic effect for removal of RhB, Mater. Lett., 275 (2020) 128099, doi: 10.1016/j.matlet.2020.128099.
[2] S. Ahmadi, L. Mohammadi, C.A. Igwegbe, S. Rahdar, A.M. Banach, Application of response surface methodology in the degradation of Reactive Blue 19 using H_2O_2/MgO nanoparticles advanced oxidation process, Int. J. Ind. Chem., 9 (2018) 241–253.
[3] J. Mittal, Permissible synthetic food dyes in India, Resonance, 25 (2020) 567–577.
[4] O. Hamdaoui, Intensification of the sorption of Rhodamine B from aqueous phase by loquat seeds using ultrasound, Desalination, 271 (2011) 279–286.
[5] S. Rahdar, A. Rahdar, M.N. Zafar, S.S. Shafqat, S. Ahmadi, Synthesis and characterization of MgO supported Fe–Co–Mn nanoparticles with exceptionally high adsorption capacity for Rhodamine B dye, J. Mater. Res. Technol., 8 (2019) 3800–3810.
[6] I. Anastopoulos, I. Pashalidis, A.G. Orfanos, I.D. Manariotis, T. Tatarchuk, L. Sellaoui, A. Bonilla-Petriciolet, A. Mittal, A. Núñez-Delgado, Removal of caffeine, nicotine and amoxicillin from (waste)waters by various adsorbents. A review, J. Environ. Manage., 261 (2020) 110236, doi: 10.1016/j.jenvman.2020.110236.
[7] K. Wang, J.H. Zhao, H.Y. Li, X.Y. Zhang, H.H. Shi, Removal of cadmium(II) from aqueous solution by granular activated carbon supported magnesium hydroxide, J. Taiwan Inst. Chem. Eng., 61 (2016) 287–291.
[8] Q. Li, X. Tang, Y.Y. Sun, Y.F. Wang, Y.C. Long, J. Jiang, H. Xu, Removal of Rhodamine B from wastewater by modified *Volvariella volvacea*: batch and column study, RSC Adv., 5 (2015) 25337–25347.
[9] D. Liu, J.L. Yin, H. Tang, H. Wang, S.S. Liu, T.T. Huang, S.S. Fang, K.X. Zhu, Z.L. Xie, Fabrication of ZIF-67@PVDF ultrafiltration membrane with improved antifouling and separation performance for dye wastewater treatment via sulfate radical enhancement, Sep. Purif. Technol., 279 (2021) 119775, doi: 10.1016/j.seppur.2021.119755.
[10] J. Liu, L.L. He, F.Q. Dong, K.A. Hudson-Edwards, The role of nano-sized manganese coatings on bone char in removing arsenic(V) from solution: implications for permeable reactive barrier technologies, Chemosphere, 153 (2016) 146–154.
[11] P.F. Xu, X.F. Shen, L. Luo, Z. Shi, Z.X. Liu, Z.G. Chen, M.F. Zhu, L.S. Zhang, Preparation of TiO_2/Bi_2WO_6 nanostructured heterojunctions on carbon fibers as a weaveable visible-light photocatalyst/photoelectrode, Environ. Sci.: Nano, 5 (2018) 327–337.
[12] L.-H. Qi, J.-D. Ding, X.-Q. Ma, X.-W. Guan, W. Zhu, H. Yao, Y.-M. Zhang, T.-B. Wei, Q. Lin, An azine-containing bispillar[5]arene-based multi-stimuli responsive supramolecular pseudo-polyrotaxane gel for effective adsorption of Rhodamine B, Soft Matter, 15 (2019) 6836–6841.
[13] Y. Shi, Q. Chang, T. Zhang, G. Song, Y. Sun, G. Ding, A review on selective dye adsorption by different mechanisms, J. Environ. Chem. Eng., 10 (2022) 108639, doi: 10.1016/j.jece.2022.108639.
[14] T. Rasheed, Magnetic nanomaterials: greener and sustainable alternatives for the adsorption of hazardous environmental contaminants, J. Cleaner Prod., 362 (2022) 132338, doi: 10.1016/j.jclepro.2022.132338.
[15] D.A. Yaseen, M. Scholz, Textile dye wastewater characteristics and constituents of synthetic effluents: a critical review, Int. J. Environ. Sci. Technol., 16 (2019) 1193–1226.

[16] J. Liu, S.Z. Wei, H.L. Zhang, Y.M. Deng, J. Baeyens, R. Dewil, N. Sweygers, L. Appels, Adsorption of acid fuchsine dye from wastewater by Mg-ferrite particles, J. Environ. Manage., 317 (2022) 115427, doi: 10.1016/j.jenvman.2022.115427.
[17] H. Daraei, A. Mittal, Investigation of adsorption performance of activated carbon prepared from waste tire for the removal of methylene blue dye from wastewater, Desal. Water Treat., 90 (2017) 294–298.
[18] C. Arora, P. Kumar, S. Soni, J. Mittal, A. Mittal, B. Singh, Efficient removal of malachite green dye from aqueous solution using *Curcuma caesia* based activated carbon, Desal. Water Treat., 195 (2020) 341–352.
[19] W.B. Yang, Y.P. Lu, F.F. Zheng, X.X. Xue, N. Li, D.M. Liu, Adsorption behavior and mechanisms of norfloxacin onto porous resins and carbon nanotube, Chem. Eng. J., 179 (2012) 112–118.
[20] S. Soni, P.K. Bajpai, D. Bharti, J. Mittal, C. Arora, Removal of crystal violet from aqueous solution using iron-based metal organic framework, Desal. Water Treat., 205 (2020) 386–399.
[21] Y.M. Hunge, A.A. Yadav, S.-W. Kang, H. Kim, Photocatalytic degradation of tetracycline antibiotics using hydrothermally synthesized two-dimensional molybdenum disulfide/titanium dioxide composites, J. Colloid Interface Sci., 606 (2022) 454–463.
[22] D. Hao, Y.F. Chen, Y. Zhang, N. You, Nanocomposites of zero-valent iron@biochar derived from agricultural wastes for adsorptive removal of tetracyclines, Chemosphere, 284 (2021) 131342, doi: 10.1016/j.chemosphere.2021.131342.
[23] M.R. Fat'hi, A. Asfaram, A. Hadipour, M. Roosta, Kinetics and thermodynamic studies for removal of acid blue 129 from aqueous solution by almond shell, J. Environ. Health Sci. Eng., 12 (2014) 62, doi: 10.1186/2052-336X-12-62.
[24] E. Sharifpour, E. Alipanahpour Dil, A. Asfaram, M. Ghaedi, A. Goudarzi, Optimizing adsorptive removal of malachite green and methyl orange dyes from simulated wastewater by Mn-doped CuO-nanoparticles loaded on activated carbon using CCD-RSM: mechanism, regeneration, isotherm, kinetic, and thermodynamic studies, Appl. Organomet. Chem., 33 (2019) e4768, doi: 10.1002/aoc.4768.
[25] P. Arabkhani, A. Asfaram, M. Ateia, Easy-to-prepare graphene oxide/sodium montmorillonite polymer nanocomposite with enhanced adsorption performance, J. Water Process Eng., 38 (2020) 101651, doi: 10.1016/j.jwpe.2020.101651.
[26] M. Sharma, J. Singh, S. Basu, Efficient metal ion adsorption and photodegradation of Rhodamine-B by hierarchical porous Fe-Ni@SiO_2 monolith, Microchem. J., 145 (2019) 708–717.
[27] J. Balamurugan, S.G. Peera, M. Guo, T.T. Nguyen, N.H. Kim, J.H. Lee, A hierarchical 2D Ni–Mo–S nanosheet@nitrogen doped graphene hybrid as a Pt-free cathode for high-performance dye sensitized solar cells and fuel cells, J. Mater. Chem. A, 5 (2017) 17896–17908.
[28] L. Yao, J.J. Yang, P.X. Zhang, L.B. Deng, In situ surface decoration of Fe_3C/Fe_3O_4/C nanosheets: towards bi-functional activated carbons with supercapacitance and efficient dye adsorption, Bioresour. Technol., 256 (2018) 208–215.
[29] H.J. Wei, J. Liu, Y. Liu, L. Wang, L.L. Li, F. Wang, X.Y. Ren, F.Z. Ren, Hollow Co-Fe LDH as an effective adsorption/catalytic bifunctional sulfur host for high-performance Lithium–Sulfur batteries, Compos. Commun., 28 (2021) 100973, doi: 10.1016/j.coco.2021.100973.
[30] J.-L. Liu, Y. Huang, J.-J. Wang, Surface-adsorbed phosphate boosts bifunctionally electrocatalytic activity of $Ni_{0.9}Fe_{0.1}S$ for hydrogen production, J. Colloid Interface Sci., 617 (2022) 525–532.
[31] J.-X. Guo, S.-Y. Wu, S.-Y. Zhong, G.-J. Zhang, G.-Q. Shen, X.-Y. Yu, Janus WSSe monolayer adsorbed with transition-metal atoms (Fe, Co and Ni): excellent performance for gas sensing and CO catalytic oxidation, Appl. Surf. Sci., 565 (2021) 150558, doi: 10.1016/j.apsusc.2021.150558.
[32] X.M. Li, J.X. Shi, X.X. Luo, Enhanced adsorption of Rhodamine B from water by Fe-N co-modified biochar: preparation, performance, mechanism and reusability, Bioresour. Technol., 343 (2022) 126103, doi: 10.1016/j.biortech.2021.126103.
[33] V.K. Gupta, S. Agarwal, R. Ahmad, A. Mirza, J. Mittal, Sequestration of toxic Congo red dye from aqueous solution using ecofriendly guar gum/activated carbon nanocomposites, Int. J. Biol. Macromol., 158 (2020) 1310–1318.
[34] A. Mariyam, J. Mittal, F. Sakina, R.T. Baker, A.K. Sharma, Fixed-bed adsorption of the dye Chrysoidine R on ordered mesoporous carbon, Desal. Water Treat., 229 (2021) 395–402.
[35] E. Abedi, M.J. Amiri, M. Sayadi, The potential use of ultrasound-assisted bleaching in removing heavy metals and pigments from soybean oil using kinetic, thermodynamic and equilibrium modeling, Environ. Sci. Pollut. Res., 28 (2021) 49833–49851.
[36] Z.G. Ren, F. Chen, B. Wang, Z.X. Song, Z.Y. Zhou, D. Ren, Magnetic biochar from alkali-activated rice straw for removal of Rhodamine B from aqueous solution, Environ. Eng. Res., 25 (2019) 536–544.
[37] T.T. Yang, Y.M. Xu, Q.Q. Huang, Y.B. Sun, X.F. Liang, L. Wang, L.J. Zhao, Adsorption characteristics and the removal mechanism of two novel Fe-Zn composite modified biochar for Cd(II) in water, Bioresour. Technol., 333 (2021) 125078, doi: 10.1016/j.biortech.2021.125078.
[38] A. He, D. He, Z. Deng, Adsorption performance of Congo red onto magnetic $Ni_{0.4}Co_{0.2}Zn_{0.4}Fe_2O_4$ nanoparticles prepared via the rapid combustion process, J. Nanosci. Nanotechnol., 19 (2019) 5914–5920.
[39] E. Mahmoudi, S. Azizkhani, A.W. Mohammad, L.Y. Ng, A. Benamor, W.L. Ang, M. Ba-Abbad, Simultaneous removal of Congo red and cadmium(II) from aqueous solutions using graphene oxide–silica composite as a multifunctional adsorbent, J. Environ. Sci., 98 (2020) 151–160.
[40] H. Chen, Y.Q. Zheng, B. Cheng, J.G. Yu, C.J. Jiang, Chestnut husk-like nickel cobaltite hollow microspheres for the adsorption of Congo red, J. Alloys Compd., 735 (2018) 1041–1051.
[41] R. Miandad, R. Kumar, M.A. Barakat, C. Basheer, A.S. Aburiazaiza, A.S. Nizami, M. Rehan, Untapped conversion of plastic waste char into carbon-metal LDOs for the adsorption of Congo red, J. Colloid Interface Sci., 511 (2018) 402–410.
[42] J. Mohanta, B. Dey, S. Dey, Highly porous iron-zirconium binary oxide for efficient removal of Congo red from water, Desal. Water Treat., 189 (2020) 227–242.
[43] L. Ren, H.X. Lin, F.C. Meng, F. Zhang, One-step solvothermal synthesis of Fe_3O_4@carbon composites and their application in removing of Cr(VI) and Congo red, Ceram. Int., 45 (2019) 9646–9652.
[44] J. Liu, N. Wang, H.L. Zhang, J. Baeyens, Adsorption of Congo red dye on $Fe_xCo_{3-x}O_4$ nanoparticles, J. Environ. Manage., 238 (2019) 473–483.
[45] M.K. Purkait, A. Maiti, S. DasGupta, S. De, Removal of Congo red using activated carbon and its regeneration, J. Hazard. Mater., 145 (2007) 287–295.
[46] J.J. Zhang, X.L. Yan, X.Y. Hu, R. Feng, M. Zhou, Direct carbonization of Zn/Co zeolitic imidazolate frameworks for efficient adsorption of Rhodamine B, Chem. Eng. J., 347 (2018) 640–647.
[47] B. Debnath, M. Majumdar, M. Bhowmik, K.L. Bhowmik, A. Debnath, D.N. Roy, The effective adsorption of tetracycline onto zirconia nanoparticles synthesized by novel microbial green technology, J. Environ. Manage., 261 (2020) 110235, doi: 10.1016/j.jenvman.2020.110235.
[48] E.C.N. Lopes, F.S.C. dos Anjos, E.F.S. Vieira, A.R. Cestari, An alternative Avrami equation to evaluate kinetic parameters of the interaction of Hg(II) with thin chitosan membranes, J. Colloid Interface Sci., 263 (2003) 542–547.
[49] Z. Wang, J.F. Su, X.F. Hu, A. Ali, Z.Z. Wu, Isolation of biosynthetic crystals by microbially induced calcium carbonate precipitation and their utilization for fluoride removal from groundwater, J. Hazard. Mater., 406 (2021) 124748, doi: 10.1016/j.jhazmat.2020.124748.
[50] J.X. Wu, X.L. Yan, L. Li, J.H. Gu, T. Zhang, L.L. Tian, X.T. Su, Z. Lin, High-efficiency adsorption of Cr(VI) and RhB by hierarchical porous carbon prepared from coal gangue, Chemosphere, 275 (2021) 130008, doi: 10.1016/j.chemosphere.2021.130008.
[51] A. Waheed, M. Mansha, I.W. Kazi, N. Ullah, Synthesis of a novel 3,5-diacrylamidobenzoic acid based hyper-cross-linked resin

for the efficient adsorption of Congo red and Rhodamine B, J. Hazard. Mater., 369 (2019) 528–538.
[52] H. Feng, Y. Nan Liang, C. Po Hu, X. Hu, Highly selective adsorption and efficient recovery of cationic micropollutants from aqueous solution via ultrathin indium vanadate nanoribbons, Sep. Purif. Technol., 293 (2022) 120952, doi: 10.1016/j.seppur.2022.120952.
[53] R.W. Abadi, C.M. Setiawan, S.P. Santoso, V. Bundjaja, A.E. Angkawijaya, Y.-F. Jiang, C. Julius Wijaya, S. Ismadji, E. Susiany Retnoningtyas, F.E. Soetaredjo, J.N. Putro, M. Yuliana, Polystyrene-templated hollow mesoporous magnetite as a bifunctional adsorbent for the removal of Rhodamine B via simultaneous adsorption and degradation, J. Environ. Chem. Eng., 10 (2022) 108194, doi: 10.1016/j.jece.2022.108194.
[54] J. Wu, J.W. Yang, G.H. Huang, C.H. Xu, B.F. Lin, Hydrothermal carbonization synthesis of cassava slag biochar with excellent adsorption performance for Rhodamine B, J. Cleaner Prod., 251 (2020) 119717, doi: 10.1016/j.jclepro.2019.119717.
[55] M.-F. Hou, C.-X. Ma, W.-D. Zhang, X.-Y. Tang, Y.-N. Fan, H.-F. Wan, Removal of Rhodamine B using iron-pillared bentonite, J. Hazard. Mater., 186 (2011) 1118–1123.
[56] W. Xiao, Z.N. Garba, S.C. Sun, I. Lawan, L.W. Wang, M. Lin, Z.H. Yuan, Preparation and evaluation of an effective activated carbon from white sugar for the adsorption of Rhodamine B dye, J. Cleaner Prod., 253 (2020) 119989, doi: 10.1016/j.jclepro.2020.119989.
[57] K. Shakir, A.F. Elkafrawy, H.F. Ghoneimy, S.G.E. Beheir, M. Refaat, Removal of Rhodamine B (a basic dye) and thoron (an acidic dye) from dilute aqueous solutions and wastewater simulants by ion flotation, Water Res., 44 (2010) 1449–1461.
[58] Y.Y. Zhang, H.J. Han, X.H. Wang, M. Zhang, Y.G. Chen, C.X. Zhai, H. Song, J.T. Deng, J. Sun, C.L. Zhang, Utilization of NaP zeolite synthesized with different silicon species and $NaAlO_2$ from coal fly ash for the adsorption of Rhodamine B, J. Hazard. Mater., 415 (2021) 125627, doi: 10.1016/j.jhazmat.2021.125627.
[59] X. Li, J. Xu, X. Luo, J. Shi, Efficient adsorption of dyes from aqueous solution using a novel functionalized magnetic biochar: synthesis, kinetics, isotherms, adsorption mechanism, and reusability, Bioresour. Technol., 360 (2022) 127526, doi: 10.1016/j.biortech.2022.127526.
[60] Y.Y. Xie, X.Z. Yuan, Z.B. Wu, G.M. Zeng, L.B. Jiang, X. Peng, H. Li, Adsorption behavior and mechanism of Mg/Fe layered double hydroxide with Fe_3O_4-carbon spheres on the removal of Pb(II) and Cu(II), J. Colloid Interface Sci., 536 (2019) 440–455.
[61] H.J. Su, Z.Q. Fang, P.E. Tsang, J.Z. Fang, D.Y. Zhao, Stabilisation of nanoscale zero-valent iron with biochar for enhanced transport and in-situ remediation of hexavalent chromium in soil, Environ. Pollut., 214 (2016) 94–100.
[62] A. Chowdhury, A.A. Khan, S. Kumari, S. Hussain, Superadsorbent Ni–Co–S/SDS nanocomposites for ultrahigh removal of cationic, anionic organic dyes and toxic metal ions: kinetics, isotherm and adsorption mechanism, ACS Sustainable Chem. Eng., 7 (2019) 4165–4176.
[63] S.P. Keerthana, R. Yuvakkumar, G. Ravi, S. Pavithra, M. Thambidurai, C. Dang, D. Velauthapillai, Pure and Ce-doped spinel $CuFe_2O_4$ photocatalysts for efficient Rhodamine B degradation, Environ. Res., 200 (2021) 111528, doi: 10.1016/j.envres.2021.111528.
[64] Y. Zhang, Q.Y. Wang, R. Li, Z.C. Lou, Y.J. Li, A novel phenolic foam-derived magnetic carbon foam treated as adsorbent for Rhodamine B: characterization and adsorption kinetics, Crystals, 10 (2020) 159, doi: 10.3390/cryst10030159.
[65] W. Huang, M. Zhang, Y.H. Wang, J. Chen, J.Q. Zhang, Biochars prepared from rabbit manure for the adsorption of Rhodamine B and Congo red: characterisation, kinetics, isotherms and thermodynamic studies, Water Sci. Technol., 81 (2020) 436–444.
[66] D. Xie, M. Zhang, F.L. Cheng, H.B. Fan, S.L. Xie, P. Liu, J.P. Tu, Hierarchical MoS_2@polypyrrole core-shell microspheres with enhanced electrochemical performances for lithium storage, Electrochim. Acta, 269 (2018) 632–639.
[67] S.F. Jia, S.F. Song, X.D. Zhao, Selective adsorption and separation of dyes from aqueous solution by a zirconium-based porous framework material, Appl. Organomet. Chem., 35 (2021) e6314, doi: 10.1002/aoc.6314.
[68] L.P. Hoang, H.T. Van, T.T.H. Nguyen, V.Q. Nguyen, P. Quang Thang, Coconut shell activated carbon/$CoFe_2O_4$ composite for the removal of Rhodamine B from aqueous solution, J. Chem., 2020 (2020) e9187960, doi: 10.1155/2020/9187960.